TECHNICAL PAPER

A numerical and experimental investigation of the effects of combination of spur dikes in series on a flow field

Shahab Nayyer[1] · Saeed Farzin[1] · Hojat Karami[1] · Mohammad Rostami[2]

Abstract

Spur dikes are used to protect river banks from erosion and also keep the main mitigation channel. Different additional structures such as "collar" and "protective spur dike" are used for reducing scouring around spur dikes. The combination of spur dike in series may be a new method to decrease scouring without using any additional structures. A computational fluid dynamic model was developed to investigate flow characteristics around triple combinational series with different shapes of spur dike (I (simple)-, L- and T-shaped). In order to verify the numerical model a (T L I) combinational series was experimented in the laboratory, and hydraulic characteristics of flow around them were measured. In this research, the numerical simulation based on optimum combination and control test is used in FLOW-3D software for analyses. In addition, several turbulence models (k–ε, RNG and LES) have been applied to achieve the best numerical simulation. The results showed that the largest flow speed, pressure, shear stress and turbulent energy in the flat bed formed close to the location of maximum scour depth and erosion. Reduction in these features helps decrease scouring and erosion. The combination of spur dike in series is a method which achieves this goal. The (L T T) series is the most effective in reducing speed, shear stress, pressure and turbulent energy around spur dikes. Actually, different geometries of spur dike, when used together, have positive effect on reducing scouring. Finally, combination of spur dikes with protective spur dike compared with series without protect. The result showed that protective spur dike can decrease intensity of flow characteristics and scour depth.

Keywords Combination of spur dike in series · Scour depth · Impermeable spur dike · Mobile bed

1 Introduction

Spur dikes are commonly used to protect coastline and river shores from scouring and erosion or to preserve in-stream hydraulic structures, such as abutment and piers. Indeed, spur dikes are among the structures that reduce the bank erosion and the ability of flow for sediment transport near the bank.

Over the last few years, studies focused on dimensional, depth and volume parameters of scouring, and also the flow characteristics around the hydraulic structures, such as spur dikes, abutment and piers. Spur dikes are often used in isolation or series. A single spur dike affects the local flow field, while spur dikes in series are often more effective to stabilize the alluvial shores. The research around this kind of obstruction has been studied widely. Mostly, research tries to present the methods for reducing the local scour and erosion and some of them determined that local scour patterns depend on the complex flow field around hydraulic structures. The results of previous work reveal that dimensions, the number

✉ Saeed Farzin
  Saeed.farzin@semnan.ac.ir

  Shahab Nayyer
  sh.nayyer@semnan.ac.ir

  Hojat Karami
  hkarami@semnan.ac.ir

  Mohammad Rostami
  mrostami2001@yahoo.com

[1] Department of Water Engineering and Hydraulic Structures, Faculty of Civil Engineering, Semnan University, Semnan, Iran

[2] Soil Conservation and Watershed Management Research Institute, Tehran, Iran

of vortices and flow field around spur dikes affect the mechanism of scour initiation and expansion [1–5].

Karami and Saneie [6] used an upstream secondary spur dike in their experiments to reduce the scour depth of the first spur dike in series. According to the results of this study, the ratio of the length of the secondary spur dike to the first spur dike was 0.5–0.58, and the most suitable distance of the main spur dike from the secondary spur dike was 1.5 to 2 times the length of the first upstream spur dike. Tang et al. [7] investigated the secondary flow around spur dikes. Their result indicated that sedimentations do not happen probably in the zone far away from the spur dike. Zhang et al. [8], Duan [9], Naji [10], Beheshti and Ataei-Ashtiani [11] and Karami et al. [12] made a variety of experiments in order to determine the flow pattern around spur dikes. Most of these works studied the effects of single spur dike. However, using series of spur dikes is more effective in protection of rivers. Ghodsian and Vaghefi [13] carried out an experimental study on flow characteristic changes and the length of the non-submerged T-shaped spur dike in a 90° bend. The results showed that the length of the spur dike affected the vortex in the separation zone. Basser et al. [14] simulated flow patterns around series of spur dikes in a rigid bed using FLOW-3D software. They found that the maximum velocity in the flow direction occurred downstream of the first spur dike and close to the tip of the spur dike. Furthermore, they found that the size and strength of the vortices in the X–Y plane (X and Y are directions of the channel length and width, respectively) within the zone between two spur dikes are larger close to the bed in comparison with the water surface.

The results of Barjastehmaleki and Hajikandi [15] indicated that when seven sacrificial piles are used in a group at a distance of 2L upstream of the tip of the spur dike, where L is the length of the spur dike perpendicular to the channel wall, the depth and volume of the scour hole are reduced, respectively, up to 30% and 60% compared with the case of single spur dike without any sacrificial piles. The numerical and experimental investigations of Safarzadeh et al. [16] on the disturbance of the flow around simple and T-shaped spur dike in flat bed showed that the increase in the length of the T-shaped spur dike in the upstream led to the disappearance of the horseshoe vortex, which was a countermeasure of scouring.

Giglou et al. [5] investigated the effect of the spur dikes on sedimentation pattern, and their results showed that increasing the angle of the spur dike from 90° to 120° increased the length and width of the sedimentation area.

Nayyer et al. [17] studied a combination of simple, L- and T-shaped spur dike in series in an erodible bed. Their results showed that the scouring of T-shaped spur dike is 0.3y (y is flow depth) less than other shapes in the first position.

Moreover, the best performance, according to lowest volume and average scour depth, is the (L T T) combination.

In another study, Nayyer et al. [18] investigated the scouring around a simple spur dike in first position under the influence of the downstream spur dikes. They fixed simple spur dike in the first position of the series with three spur dikes and changed the second- and third-position spur dikes. The results showed that scouring depth for simple spur dike (I-shaped) in the first position is about 2.7y (y is flow depth). They suggested the (I T L) series as the best and optimal performance between all combinations of that study. The mean scouring depth for this optimal series in the longitudinal section of flume is equal to 0.02y. Vaghefi et al. [19] simulated the T-shaped spur dike in the presence of attractive and repelling protective spur dikes. Their results indicated that the maximum shear stress in different modes of protective spur dike increases 20.55% on average.

The 3D flow field around a series of spur dikes is complex because of the interactions between flow and sediment transition as the scouring develops. Methods for predicting the 3D flow field have been developed through the software of 3D hydrodynamic models such as FLOW-3D. In this study, the commercial CFD software FLOW-3D was selected.

The aim of this research is to investigate the effect of a combination of spur dikes in series on flow characteristics of the flat and eroded bed surface. The simulation results are verified with experimental data obtained at the Soil Conservation and Watershed Management Research Institute (SCWMRI) of the Agricultural Research and Education Organization (AREO) in Tehran. This paper presents the simulated results of different combinations of spur dikes in series, which are based on experimental measurements, and compares the results to the same measurements. In addition, the optimal combination is simulated in the presence of a protective spur dike in order to investigate the effect of this structure on main spur dikes.

2 Materials and methods

2.1 Experimental procedure

The experiment was performed in a flume 14 m long, 1.5 m wide and 0.6 m tall located at the SCWMRI[1] of AREO[2] in Tehran. This flume was supported by a steel frame, and the channel sides were made with smooth Plexiglas. Threshold condition according to Shields [20] is the condition in which the sediment transport rate is equal to zero. Equations 1–4

---

[1] The Soil Conservation and Watershed Management Research Institute.

[2] The Agricultural Research and Education Organization.
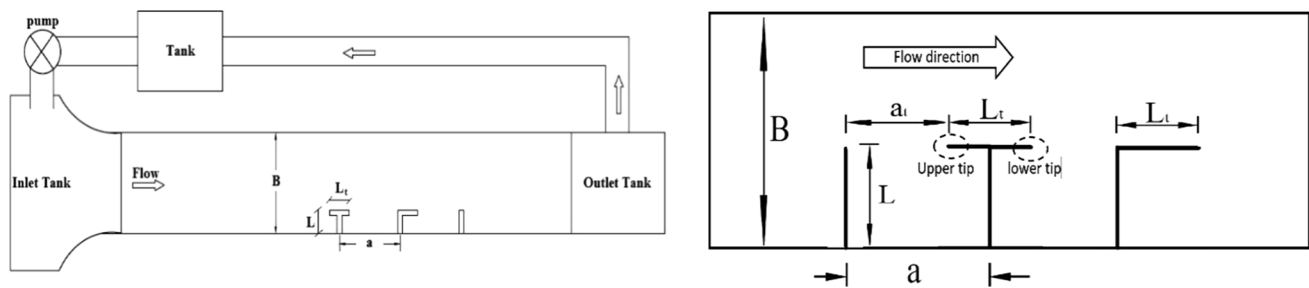
Fig. 1 Plan view of the experimental setup and geometry of spur dikes

are used to calculate the Shields parameter and critical velocity to achieve discharges.

$$\theta_{cr} = \frac{\tau_{b,cr}}{(\rho_S - \rho) \cdot g \cdot d_{50}}, \tag{1}$$

$$Re_* = \frac{U_{*,cr} \cdot d}{\upsilon}, \tag{2}$$

$$u_{cr} = \frac{u_{*,cr} \cdot C}{\sqrt{g}}, \tag{3}$$

$$C = f(d, K_s, \upsilon, u_{*,cr}), \tag{4}$$

where ($\tau_{b,cr}$) is the bed critical shear stress, (θ_{cr}) is the critical Shields parameter, (g) is gravity, (d_{50}) is mean sediment size, (ρ) and (ρ_s) are flow and sediment density, respectively, ($U_{*,cr}$) is critical shear velocity, (υ) is water Kinematic viscosity, (d) is flow depth, (C) is Chezy coefficient, and (k_s) is equivalent roughness. Considering the motion threshold condition ($u/u_{cr} = 0.95$) for the sediment bed and using the same Shields parameter in all experiments, the discharge was found to be 28.5 L per second. Thus, the flow depth (y) was set to 6 cm in terms of discharge, laboratory channel dimensions and bed motion conditions. The bed materials were natural river sand with uniform granularity, where the median sand diameter of sediment and geometric deviation of the substrate particles were $d_{50} = 1$ mm and $\sigma_g = 1.41$, respectively. The geometries of the spur dikes used were simple, L-shaped and T-shaped. Three spur dikes with $L = 35$ cm length (gives an obstruction of $L/B = 23\%$), 4 mm thickness and 30 cm height, made with Plexiglas, were established on one side of the channel with a distance of 105 cm ($a = 3L$ where L is the length of spur dike). The web and wing of the spur dike are equal ($L/L_t = 1$) (Fig. 1).

Changes in scour depth on the erodible bed were measured at a precision of 1 mm during the test time with a bed profiler device. The P-EMS[3] was used to measure velocity on the rigid bed in the longitudinal (u) and lateral (v) flow directions. The electromagnetic velocity meter measures two-directional water velocity in two perpendicular directions. The measurement principle is based on a conductive fluid moving through a magnetic field.

The duration of the tests on the erodible bed was 5 h to allow the erosion to reach more than 85% of equilibrium scour depth [17]. Tests were planned for all combinations using simple, L- and T-shaped spur dikes in series of three spur dikes. After the eroded bed reached the eroded state, total bed changes were measured. The number of measurement points for flow velocities was 168 on the x–y plane at three levels: close to the bed, center and surface of the flow as indicated in Fig. 2.

2.2 Numerical model

FLOW-3D is a general-purpose computational fluid dynamics (CFD) software. It employs specially developed numerical techniques to solve the equations of motion for fluids to obtain transient, three-dimensional solutions to multi-scale, multi-physics flow problems. An array of physical and numerical options allows users to apply FLOW-3D to a wide variety of fluid flow and heat transfer phenomena. This commercial software has been used for diverse hydraulic and coastal engineering applications, such as flow and erosion around a pier [21], flow over a sharp-crested spillway and the near shore transformation of waves [22, 23]. The governing equations on fluid flow are mass continuity and momentum equations. The general form of mass continuity equation is,

$$V_F \frac{\partial \rho}{\partial t} + \frac{\partial}{\partial x}(\rho u A_x) + \frac{\partial}{\partial y}(\rho v A_y) + \frac{\partial}{\partial z}(\rho w A_z) = 0 \tag{5}$$

Three-dimensional forms of the momentum equations can be written as:

---

[3] Two-dimensional accelerometer programmable electromagnetic liquid velocity meter.
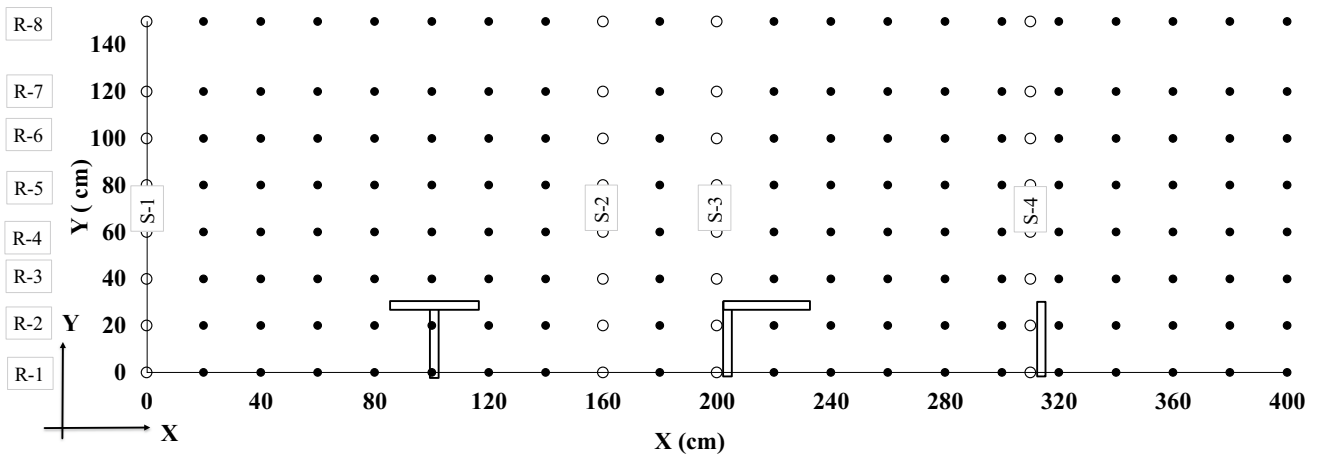
Fig. 2 Position of spur dikes and the velocity profile measuring points on the rigid bed

$$\frac{\partial u}{\partial t} + \frac{1}{V_F}\left\{ uA_x\frac{\partial u}{\partial x} + vA_y\frac{\partial u}{\partial y} + wA_z\frac{\partial u}{\partial z} \right\} = -\frac{1}{\rho}\frac{\partial p}{\partial x} + G_x + f_x - b_x,$$

$$\frac{\partial v}{\partial t} + \frac{1}{V_F}\left\{ uA_x\frac{\partial v}{\partial x} + vA_y\frac{\partial v}{\partial y} + wA_z\frac{\partial v}{\partial z} \right\} = -\frac{1}{\rho}\frac{\partial p}{\partial x} + G_y + f_y - b_y,$$

$$\frac{\partial w}{\partial t} + \frac{1}{V_F}\left\{ uA_x\frac{\partial w}{\partial x} + vA_y\frac{\partial w}{\partial y} + wA_z\frac{\partial w}{\partial z} \right\} = -\frac{1}{\rho}\frac{\partial p}{\partial z} + G_z + f_z - b_z,$$

$$(6)$$

where V_F is the fractional volume open to flow, ρ is fluid density, u, v, w, are velocity components in x, y, z directions, and A_x, A_y and A_z are the fractional area open to flow in x, y, z directions. G, f and b are, respectively, body acceleration, viscous acceleration and flow losses in porous media or across porous baffle plate [24].

2.2.1 Simulation domain

The simulation domain is constructed in FLOW-3D by establishing solid geometric objects to determine the flow zone for a simulation. There are two numerical techniques available.

1. VOF[4] method:

    The VOF method is used when there is free surface flow. In this method, to define the water surface profiles, a function $f(x, y, z)$ is used according to Eq. (9),

$$\frac{\partial F}{\partial t} + u_j\frac{\partial F}{\partial x_j} = 0, \qquad (9)$$

where f function is the index of volume percentage of water phase in a cell; it ranges between zero and one.

This function is equal to one if the cell is full of water; in case the cell is full of air, f is equal to zero; and in other situations there is free water surface in the cell [25, 26].

2. Fractional Area-Volume Obstacle Representation (FAVOR) method:

This method computes the open area fractions on the cell faces along with the open volume fraction and reconstructs the geometry based on these parameters. This approach offers a simple and accurate way to represent complex surfaces in the domain without requiring a body-fitted grid.

In the present study, all simulations were continued until the flow reached the steady state. Experimental data from the control test were used to calibrate and evaluate simulation results from FLOW-3D. Bed changes and the topography of the eroded bed measured in the experiments were simulated as a rigid bed in FLOW-3D.

RNG K-ε, standard K–ε and LES turbulence models were used for simulation of the flow field around the spur dikes, and the results compared with the experimental data.

Boundary conditions were set at the different boundaries. At entrance of the channel (X_{min}), "volume flow rate" has been used. For walls and bed, (Y_{min}, Y_{max}, Z_{min}), boundary
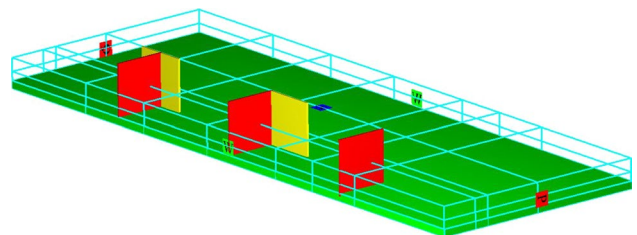

Fig. 3 A schematic view of boundaries and mesh planes used in the numerical model
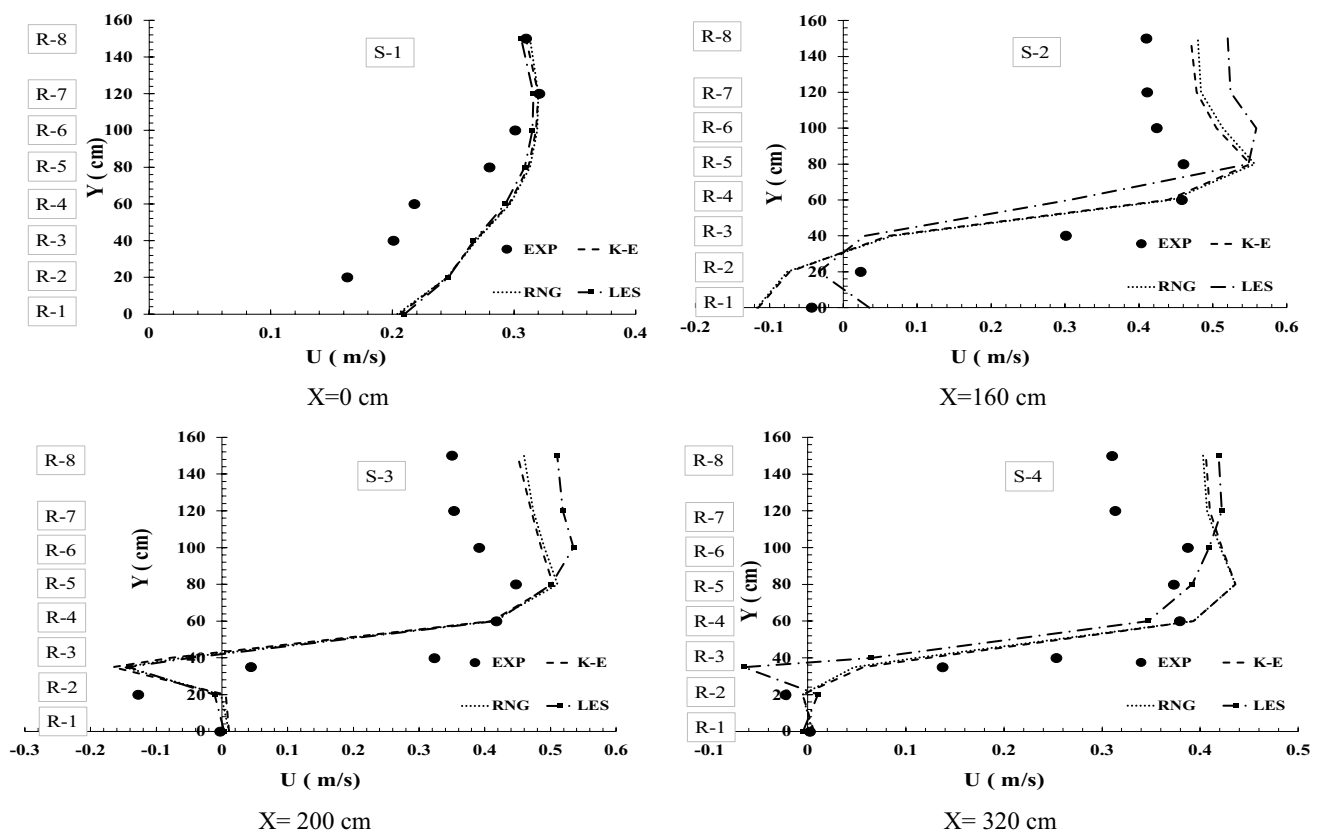
---

[4] Volume of fluid.

Fig. 4 Verification of longitudinal flow velocity in numerical model using experimental data for sections with no filled circle point in Fig. 2, near the bed (Z = 1 cm)

condition of "wall" have been defined. In upper (free surface) and exit boundary, (Z_{max} and X_{max}), "symmetry" and "specified pressure" have been used, respectively. The mesh planes and boundaries are shown in Fig. 3.

As shown in Fig. 3, several mesh planes were used to increase simulation accuracy in the vicinity of spur dikes and bed. The total number of mesh cells in the longitudinal, lateral and vertical directions is equal to 298, 102 and 26, respectively. Also, the maximum aspect ratio in all directions is equal to 1.

In order to verify the longitudinal and lateral velocity statistics quantities such as the coefficient of determination (R^2), root-mean-square error (RMSE), mean absolute error (MAE) and mean square error (MSE) are used. These are defined according to,

where p and o are prediction and observation velocity values, respectively.

3 Results and discussion

In this section, the effect of spur dikes with different geometries on the flow field characteristics, for the flat and eroded bed, has been investigated numerically. The effect of a protective spur dike on the optimal spur dike series is studied.

$$R^2 = 1 - \left[\frac{\sum_{i=1}^{N}(O-P)^2}{\sum_{i=1}^{N}O^2 - \left(\frac{\sum_{i=1}^{N}P^2}{N}\right)} \right], \quad \text{RMSE} = \sqrt{\frac{\sum_{i=1}^{N}(O-P)^2}{N}}, \quad \text{MAE} = \frac{1}{N}\sum_{i=1}^{N}|O-P|, \quad \text{MSE} = \frac{1}{n}\sum_{i=1}^{N}(O-P)^2$$

Table 1 Statistical comparison of longitudinal and lateral velocities for the experimental and numerical results on the flat bed case

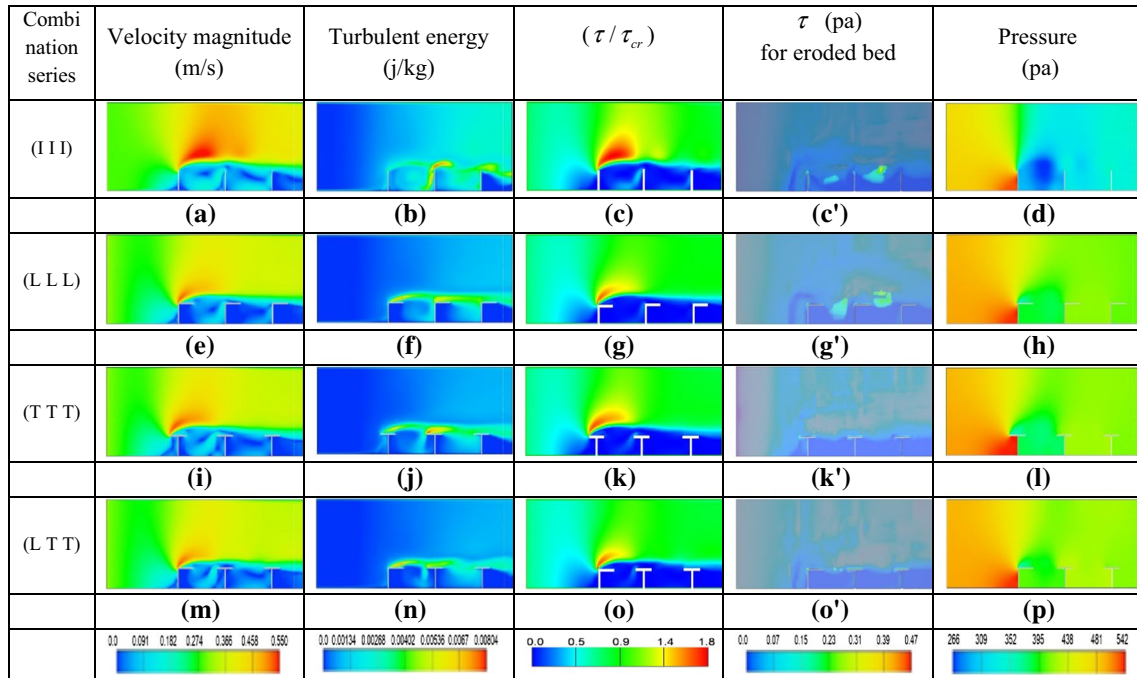| Turbulence model	Longitudinal flow velocity (u) error				Lateral flow velocity (v) error			
	R^2	RMSE	MAE	MSE	R^2	RMSE	MAE	MSE
RNG k–ε	0.822	0.128	0.088	0.0163	0.696	0.067	0.041	0.0045
K–ε	0.833	0.127	0.085	0.0160	0.727	0.062	0.039	0.0038
LES	0.771	0.143	0.101	0.0204	0.568	0.08	0.053	0.0063

Fig. 5 Distribution of x-velocity, turbulent energy and shear stress for different combinations on flat bed

3.1 A comparison between numerical and experimental results

The simulation results for the plane of the flatbed around the (T L I) combination of spur dike in series were compared with the experimental measurement in order to verify the numerical data.

The longitudinal flow velocity (u) at different sections for three turbulent models and experimental results, near the bed ($Z = 1$ cm), are shown in Fig. 4. The standard k–ε turbulent model has reasonable conformity with experimental results. Secondary flows near the adjacent shore and in the vicinity of spur dikes are formed. Near the opposite shore, the flow velocity values at different sections are closer to each other.

The errors for different turbulence models with respect to experimental data are presented in Table 1. Discrepancies are indicative of, according to Table 1, the best turbulence model for simulation of mean longitudinal and lateral velocities in the k–ε model. Therefore, the K–ε model is chosen for the comparative study of the simulated and experimental results of the flow pattern around the spur dikes.

3.2 Flow characteristics

Different combinations with three spur dikes in series were designed using simple, L- and T-shaped spur dikes in laboratory. The control combination was (I I I), (L L L) and (T T T) series for scouring and erosion investigation. The (L T T) series was suggested as the optimum composition according to less scour depth and erosion volume [17]. Therefore, in order to investigate the flow pattern, the control and optimum configuration were simulated. Simulations were performed for an initially flat bed.

As can be observed in Fig. 5, the computed distribution of velocity, turbulent energy, dimensionless shear stress and pressure are depicted for different series.

It is evident that for all combinations, flow velocity before the spur dikes range has constant distribution in channel width, but changes in velocity value initiate with cross section constriction. Weak vortex is formed in the upstream of the first spur dike in the vicinity of wall. The maximum velocity is located in front of spur dikes, but developed from tip of the wing of first spur dike. Flow

Fig. 6 Comparison of mobile bed variations for control and optimum experimental tests

(I I I) series

(L L L) series

(T T T) series

(L T T) combinational series

Min   Max
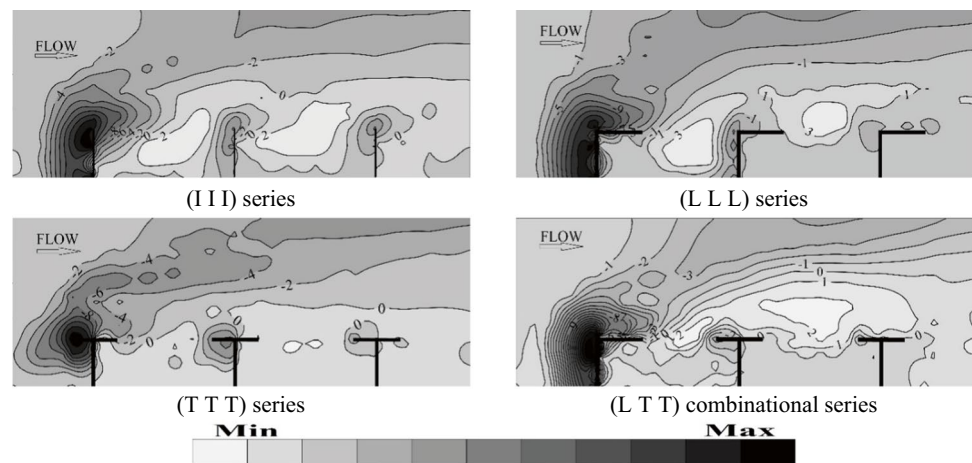
field between simple spur dikes in (I I I) series (Fig. 5a) has greater velocities than the other geometries in this area. The (L T T) series (Fig. 5m) has smaller velocities than the other geometries, especially between the first and second spur dikes; this is due to the proximity of the first and second spur dikes' wing tips and decrease in flow in this limited area.

A comparison of the turbulence energy for different series indicated that the L-shaped spur dike has an effect of reducing the turbulent energy around the downstream spur dikes. This surprising effect is clear for the turbulence energy value of the second spur dike in (L T T) series in comparison with the (T T T) series (Fig. 5j, n).

Investigation of bed shear stress distribution can help to predict the initiation point of scouring and erosion range. The experimental and numerical results for mobile bed showed that the maximum amount of scour occurs at the same location of maximum velocity and shear stress. As shown in Fig. 5g, o, for τ/τ_{cr}, the L-shaped spur dike in the first position has less area of high shear stress than the other geometries near the tip of the spur dike. This result can indicate the cause of the low scour around the L-shaped spur dike. The maximum shear stress area developed in front of the spur dikes causes erosion on the main channel.

Critical shear stress according to the channel dimension and hydraulic characteristics of flow was calculated to be 0.502 Pa. Shear stress for equilibrium eroded bed is shown in Fig. 5c', g', k', o'. These figures show that after scouring and erosion, the bed reaches the equilibrium and after this, the shear stress in the channel tends to the lower amount than the critical shear stress value, which indicates that erosion and scouring reduced and then ceased.

The flow impacts with the spur dike at the upstream side; therefore, the velocity head changes to the pressure head and the bed scouring occurs due to horseshoe and wake vortices. The maximum pressure range on the upstream of the T-shaped first spur dike (Fig. 5l) is larger than the other geometries, which causes to make widest upstream scour hole. This result demonstrates agreement with measured hole dimensions in experimental tests.

Bed change in experimental tests is depicted in Fig. 6. According to this figure, the maximum scour depth occurs at the tip of the nose of the first spur dike, which is located in the range of maximum velocities, turbulent energy, bed shear stress and pressure. Based on those investigations, observed flow characteristic values on the solid flat bed can help predict scour hole and erosion range on the mobile bed.

3.3 Streamlines

Figures 7 and 8 show streamlines for combination of spur dikes in series with eroded bed. The presence of spur dikes leads the flow to the opposite side and compresses the flow, so because of flow continuity the velocities increase.

The impact of flow with spur dike causes formation of horseshoe and wake vortices upstream of the spur dikes, as shown in Fig. 7. These vortices for simple and L-shaped geometries are almost the same. However, the T-shaped spur dike has a different vortex formed in the horizontal plane. The horizontal vortex develops upstream and causes wide bed erosion. Although the local scour depth for this geometry is smaller, the scour hole is larger than for other geometries.

The vortex formed between spur dikes is the main reason for sedimentation in this area. According to the geometry of the adjacent spur dikes, a vortex is created in different shapes. Wing length (L_t) and distance of tips of spur dikes between two consecutive spur dikes (a_t) are determinant for the shape of the vortex. Therefore, sedimentation varies in form and volume.

It is visible from Fig. 7 that the generated vortices have a significant impact on the flow field. Thus, it is impossible to ignore the effect of the downstream spur dike on the

Fig. 7 Variation of streamlines along the channel around the spur dikes for control and optimum experimental tests on eroded bed

(I I I) series

(L L L) series
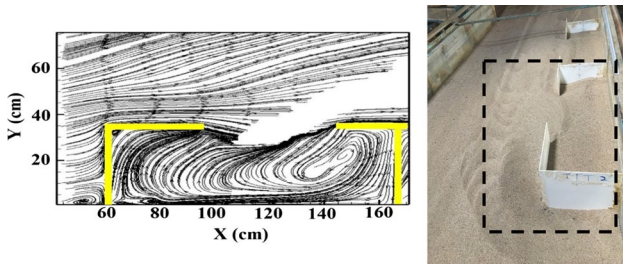
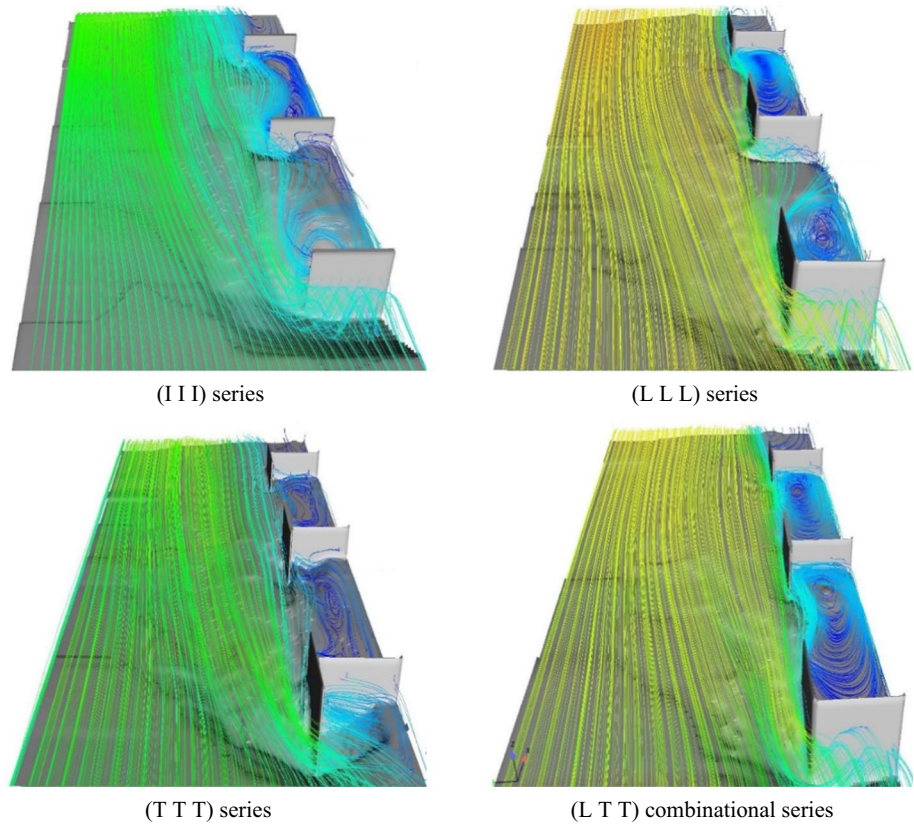(T T T) series

(L T T) combinational series

Fig. 8 Streamline in *X–Y* directions around the first and second spur dikes of (L T T) series on bottom of eroded bed

scouring of the upstream spur dike. Moreover, the rotational flow range between the first and second spur dikes in I I I, L L L and T T T combinations is affected by outer flow, which makes it easier for the flow to enter the area between spur dikes from the outside.

For the (L T T) combination of spur dikes in series it is evident that the a_t between first and second spur dikes is smaller than the other series, and the vortex in this area is totally limited and less affected than the other series. So entrance of active stream to spur dikes scope

decreases. The lack of entry of active flow with sediment into the area between the first and second spur dikes in L T T combination causes the major sedimentation near the tip, which ultimately decreases the depth of erosion in the lower tip of the first spur dike and the tip upstream of the second spur dike. The reason for the low scour depth in the L T T combination was the same. Actually because the tips of spur dikes are close to each other (a_t) (according to Fig. 8), the bed sediment of the first spur dike enters the scour hole of the second spur dike and fills it. This continues until inflow and outflow of sediment reach equilibrium.

3.4 Effect of a protective spur dike on the optimal series: configuration (L T T)$_p$

Experimental investigation of Karami et al. [12] on the effect of a protective spur dike (SD$_p$) located upstream of the first spur dike indicated that an appropriately designed protective spur dike (SD$_p$) is able to decrease the average of the maximum scour depth around the main spur dikes. They identified a protective spur dike (SD$_p$) with an angle θ of 45° or 90°, a relative length of $L_p/L = 0.6$ and a relative spacing of $X/L = 2$ or 2.5 as the optimum parameters (θ and L_p are angle and length of protective spur dike (SD$_p$)
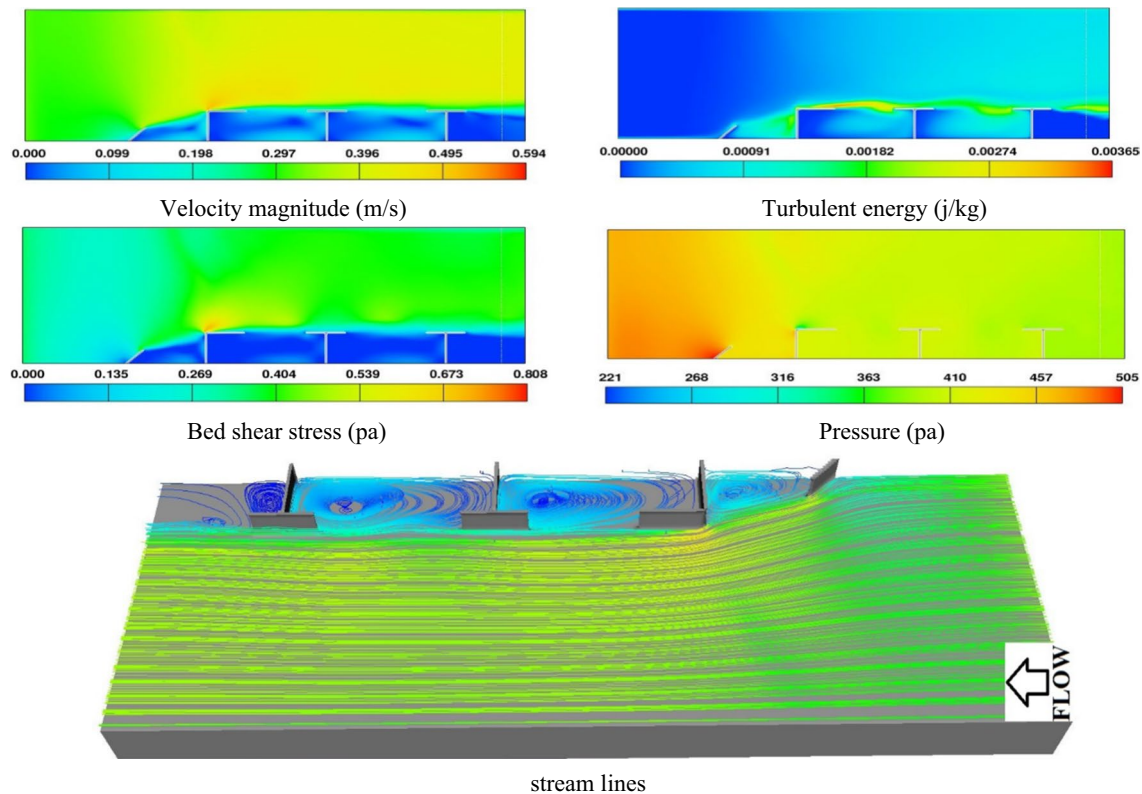
Fig. 9 Hydraulic characteristic for $(L\ T\ T)_P$ series in the presence of protective spur dike (SD_p)

and X is the distance between protective spur dike (SD_p) and the first main spur dike).

According to their results, and for the investigation of the effect of (SD_p) on the optimal combination of the present study, a (SD_p) was defined with $\theta = 45°$, $L_p/L = 0.6$ and $X/L = 2$. Figure 9 depicts the simulation results for this situation and indicates that (SD_p) has an effective influence on the flow field. Velocity magnitude considerably reduced around the first spur dike, while a small area of high velocity occurred near the tip of the first spur dike. According to a gradual constriction, velocity magnitude decreases on the main flow direction. Turbulent energy reduced but formed in the vaster area than the $(L\ T\ T)$ series.

The bed shear stress and pressure amount around the main spur dikes decreased, which helps reduce the scour depth.

Consequently, according to the results of Sect. 3.3, maximum scour is located in the vicinity of maximum values of velocity magnitude, shear stress and turbulent energy, so with (SD_p) these values are reduced, which helps reduce scour and erosion range. In addition, erosion range formed far from the main spur dikes.

4 Conclusion

The combination of spur dikes in series can be a new method to reduce scouring without using any additional structure. This method evaluated scouring and flow features. To simulate the three-dimensional flow around a series with three spur dikes on the flat and eroded bed in the rigid situation, this study applied FLOW-3D software. Simple, L- and T-shaped spur dikes were used in the combination. The (T L I) series combination was measured in the laboratory for comparison and verified using numerical model results. According to the results of Nayyer et al. [17], the optimum combination for minimum scour depth and erosion is the (L T T) series. This combination was compared to control tests (I I I, L L L, T T T) using simulation. The main results of this investigation are as follows:

- Assessing experimental data and numerical results demonstrated that FLOW-3D software is a model with reasonable accuracy in terms of simulating the flow field around spur dikes. The k–ε turbulence model with $R^2 = 0.78$, RMSE $= 0.0945$, MAE $= 0.062$ and MSE $= 0.0133$ has good conformity with experimental data.

- The velocity magnitude in the (L T T) series is smaller than the other combinations, especially between the first and second spur dikes. This is owing to the proximity of the first and second spur dikes' wing tips (lowest a_t) and decreasing flow entrance in this limited area.
- The L-shaped spur dike in the first position has smaller area of high shear stress and turbulent energy than the other geometries near the tip of the spur dike and also has a positive effect on downstream spur dikes, especially on the T-shaped spur dike.
- Flow pressure area of the upstream of the L-shaped spur dike located in the first position has lower width than that of the T-shaped spur dike. This phenomenon can help reduce scour hole area and consequently decrease erosion volume.
- Locations of the maximum velocity, pressure, turbulent energy and shear stress in flat bed are in the vicinity of the location of the maximum scour depth and erosion. Based on this result, flow characteristic values on the solid flat bed can help predict scour hole and erosion range on a mobile bed.
- Maximum amount of shear stress in the eroded bed is lower than the calculated critical shear stress, which gives rise to an equilibrium bed without erosion.
- Streamlines indicated that a horizontal vortex formed upstream of the T-shaped spur dike and can create a wide erosion area for this geometry. This area for first spur dike formed in the location of the maximum scour depth on the mobile bed, which causes maximum erosion volume for this geometry. Vortex between consecutive spur dikes formed with weak strength and caused sedimentation in this area. Because of the proximity of tip of wings (low a_t), the vortex between the L- and T-shaped spur dikes is more limited than the other geometries. This closeness helps reduce scour depth and sedimentation.
- A protective spur dike located upstream of a main spur dike leads to reduction in the maximum values of flow characteristics, far from the main spur dikes. Consequently, this helps reduce the maximum scour depth and erosion.

References

1. Neill CR (1973) Guide to bridge hydraulics. Roads and Transportation Association of Canada, University of Toronto Press, Toronto
2. Zaghloul NA (1983) Local scour around spur-dikes. J Hydrol 60:123–140
3. Fathi A (1992) Study of scouring around groynes. M.Sc. Thesis, Tarbiat Modarres University, Tehran, Iran
4. Van Rijn LC (1993) Principles of sediment Transport in Rivers. Estuaries and Coastal Seas and Oceans. Delft Hydraulics Publications
5. Giglou AN, Mccorquodale JA, Solari L (2017) Numerical study on the effect of the spur dikes on sedimentation pattern. Ain Shams Eng J 9(4):2057–2066
6. Karami H, Saneie M (2005) Experimental investigation on the effect of secondary length spur dike on scouring spur dikes. M.Sc. Thesis, Amir Kabir University, Iran
7. Tang XL, Xiang DING, Chen ZC (2007) Experimental and numerical investigations on secondary flows and sedimentations behind a spur dike. J Hydrodyn 19(1):23–29
8. Zhang H, Nakagawa H, Ishigaki T, Muto Y (2005) Prediction of 3D flow field and local scouring around spur dykes. J. Hydraul Eng 49:1003–1008
9. Duan JG (2006) Three-dimensional mean flow and turbulence around a spur dike. In: Proceedings of Hydraulic Engineering, ASCE
10. Naji Abhari M (2010) Experimental and numerical simulation of flow in a 90° bend. Flow Meas Instrum 21:292–298
11. Beheshti AA, Ataei-Ashtiani B (2010) Experimental study of three-dimensional flow field around a complex bridge pier. J Eng Mech 136(2):143–154
12. Karami H, Ardeshir A, Behzadian K, Ghodsian M (2011) Protective spur dike for scour mitigation of existing spur dikes. J Hydraul Res 49(6):809–813
13. Ghodsian M, Vaghefi M (2009) Experimental study on scour and flow field in a scour hole around a T-shape spur dike in a 90° Bend. Int J Sedim Res 24(2):145–158. https://doi.org/10.1016/S1001-6279(09)60022-6
14. Basser H, Ardeshir A, Karami H (2012) Numerical simulation of flow pattern around spur dikes series in rigid bed. In: 9th International congress on civil engineering, Isfahan University of Technology (IUT), Isfahan, Iran
15. Barjastehmaleki S, Hajikandi H (2015) Experiments on the arrangement and location of sacrificial piles to reduce erosion around spur dikes. In: The 1st international conference on civil engineering, architecture and urban economy development, Shiraz, Iran
16. Safarzadeh A, Salehi Neyshabouri SAA, Zarrati AR (2016) Experimental investigation on 3D turbulent flow around straight and T-shaped spur dikes in a flat bed channel. J Hydraul Eng 142(8):04016021
17. Nayyer S, Farzin S, Karami H, Rostami M (2018) Experimental study of the effect of spur dike's different shapes on time variation of scour depth around them. Irrig Drain Struct Eng Res J 72(19):33–50
18. Nayyer S, Karami H, Farzin S, Rostami M (2018) Experimental study of scouring around a simple spur dike under the influence of adjacent spur dikes. Iran J Irrig Drain 12(4):840–849
19. Vaghefi M, Faraji B, Akbari M, Eghbalzadeh A (2018) Numerical investigation of flow pattern around a T-shaped spur dike in the vicinity of attractive and repelling protective structures. J Braz Soc Mech Sci Eng 40(2):93–107
20. Shields A (1936) Application of similarity principles and turbulence research to bed-load movement. Hydrodynamics Laboratory Publications. No. 167 (trans: Ott WP, van Uchelen JC). U.S. Department of Agriculture Soil Conservation Service Cooperative Laboratory, California Institute of Technology, Pasadena, Calif (Cited in Buffington 1999)
21. Richardson JE, Panchang VG (1998) Three-dimensional simulation of scour-inducing flow at bridge piers. J Hydraul Eng 124(5):530–540
22. Bradford SF (2000) Numerical simulation of surf zone dynamics. J Water Port Coastal Ocean Eng 126(1):1–13

23. Chopakatla SC (2003) A CFD model for wave transformations and breaking in the surf zone. M.Sc. Thesis, Ohio State University, Columbus, Ohio

24. Flow Science Inc (2008) FLOW-3D User's Manual, 9.3 ed. Flow Science Inc, Los Alamos

25. Hirt CW, Nichols BD (1981) Volume of fluid (VOF) method for the dynamics of free boundaries. J Comput Phys 39(1):201–225

26. Hirt CW, Chen KS (1996) Simulation of slide-coating flows using a fixed grid and a volume-of-fluid front-tracking technique: startup and bead breakup (No. SAND-96-0443C; CONF-960225-1). Sandia National Labs, Albuquerque, NM, USA